Exploration Geophysics (2004) ***35****, 217–223*

In-situ stress field and fault reactivation in the Mutineer and Exeter Fields, Australian North West Shelf

Adrian White[1] **Richard Hillis**[2]

Key Words: Mutineer and Exeter fields, in-situ stress field, geomechanical modelling, fault reactivation, Australian North West Shelf

ABSTRACT

This study evaluates the in-situ stress field and the potential risk of fault reactivation and seal breach in the Mutineer and Exeter fields, Australian North West Shelf. Stress determinations are undertaken using pumping pressure test, rock mechanical, and log data from twelve wells. Subsequent geomechanical modelling uses the stress data to assess pore pressure changes that may induce slip on mapped faults cutting the region.

The principal stresses are assumed to be the vertical stress (S_V), and a maximum and minimum horizontal stress, S_H and S_h respectively. Borehole breakouts and drilling-induced tensile fractures (DITFs) interpreted from image logs indicate S_H has an average orientation of 107°N and S_h is orientated 017°N. Leak-off test data compiled from well completion reports reveal the magnitude of S_h increases with depth at a rate of 17.1 MPa/km. Density log data show S_V can be approximated by a power law function. An upper bound to S_H is calculated using the frictional limit to stress beyond which faulting occurs when using a frictional coefficient of 0.6. Better constraints on the magnitude of S_H are gained using rock mechanical data, knowledge of S_h and S_V, mud weights, and the occurrence of borehole breakouts and DITFs. Stress magnitudes show that the tectonic regime is strike-slip ($S_h < S_V < S_H$).

The likelihood of fault reactivation in Mutineer-Exeter is expressed as the increase in pore pressure required for fault slip. Results show that faults are non-optimally orientated for reactivation by the stress field. The likelihood of brittle seal failure due to fault reactivation is low, primarily because of non-optimally orientated faults. The creation of new faults requires greater increases in pore pressure than reactivation and is thus seen as being more unlikely. The results have implications for seal integrity, well bore stability, and the safe and successful production of the fields.

INTRODUCTION

During the life of hydrocarbon fields, brittle failure of reservoirs and rocks in their vicinity may arise. A well-documented example of such failure occurred during the production of the Ekofisk Field in the Norwegian North Sea (Teufel et al., 1991). Brittle failure can have positive implications for production, namely the increase in fracture permeability thus aiding the extraction of hydrocarbons. However, pore pressure (P_p) drawdown can have negative effects. Reducing pore pressure may induce casing failure with the results being well bore destabilisation and damage to production infrastructure (Streit and Hillis, 2002).

Quantification of the in-situ stress field and geomechanical analyses conducted on faults is undertaken for the Mutineer and Exeter fields. The fields are located within the Carnarvon Basin on the Australian North West Shelf (Figure 1). Exeter lies approximately 150 km N of Dampier in Western Australia while Mutineer is located a further 10 km to the NE. Both fields are situated on the NE–SW trending, fault bounded, Rankin Platform. The reservoir unit is the Jurassic-age Angel Formation, the top of which occurs at approximately 3100 metres TVDSS. The orientations and magnitudes of the in-situ stresses are determined using data from 12 vertical pre-production wells drilled between 1978 and the end of 2002. Stress orientations are resolved from borehole breakouts and drilling-induced tensile fractures (DITFs) seen on image logs (Figures 2 and 3). These features show the orientation of the maximum and minimum horizontal stresses, S_H and S_h. Pumping pressure test and wireline log data quantify the magnitudes of the minimum horizontal stress and the vertical stress while a combination of modelled and measured data constrains the maximum horizontal stress.

The threat of damage to wells and the reservoir can be minimised by considering the critical changes in pore pressure likely to cause reactivation of existing faults or the creation of new ones. Geomechanical modelling is undertaken to assess the risk of reactivation of faults cutting Mutineer-Exeter. Modelling

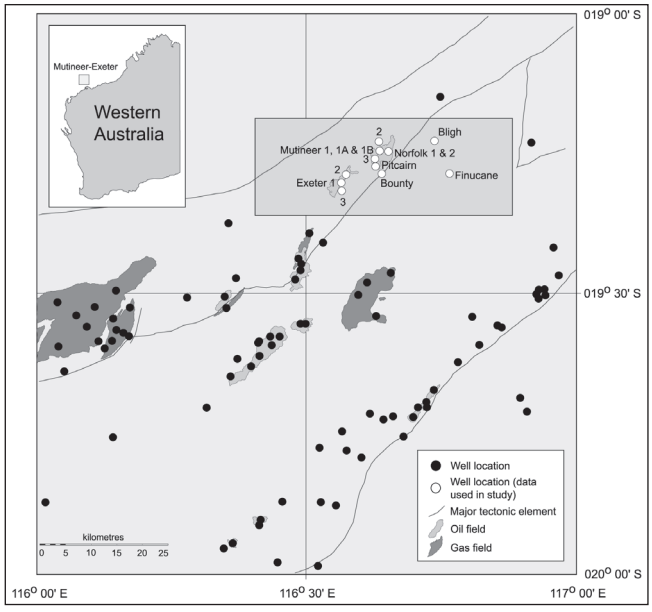

Fig. 1. The location of the Mutineer and Exeter fields.

[1] *Australian School of Petroleum*
The University of Adelaide
SA 5005, Australia
Tel: +61 8 8303 4293
Fax: +61 8 8303 4345
Email: awhite@asp.adelaide.edu.au

[2] *Australian School of Petroleum*
The University of Adelaide
SA 5005, Australia
Email: rhillis@asp.adelaide.edu.au

Manuscript received 23 January, 2004
Revised manuscript received 1 July, 2004

particularly focuses on those faults that impact on the reservoir rocks (the Angel Formation) and the sealing shale lithologies (the Muderong Formation and underlying Forestier Formation). Geomechanical modelling requires knowledge of the stress field (orientations and magnitudes), pore pressures, orientations and dimensions of faults, and the frictional properties and the strengths of rocks and fault planes.

PORE PRESSURES

Pore pressure (P_p) measurements have been conducted in seven wells in Mutineer-Exeter. Measurements are restricted to repeat formation tests (RFTs) recorded within the reservoir (Figure 4). Those data available indicate that pore pressures are hydrostatic within the reservoir and that hydrostatic pressures persist in both hanging walls and footwalls of faults. Drilling mud weight data can be considered a proxy for P_p in the upper 3 km to develop a better understanding of the P_p profile. Mud weights used in the drilling of Mutineer-Exeter are only slightly in excess of the hydrostat and therefore indicate that the region is normally pressured. Therefore, a hydrostatic regional P_p profile (10 MPa/km) was assumed for the geomechanical modelling.

STRESS ORIENTATIONS

The principal stresses are assumed to be the vertical stress (S_V) and a maximum and minimum horizontal stress, S_H and S_h. Orientations of S_H and S_h can be determined from the output of a number of downhole tools. Formation Micro-Imager (FMI) logs and caliper logs were interpreted for well Mutineer 1b. The "image" of the well bore wall produced by the FMI tool is based on the relative resistivity/conductivity of the wall rocks. Calipers measure the dimensions of the borehole and the azimuth of the measurement. They can reveal borehole ellipticity together with the orientation.

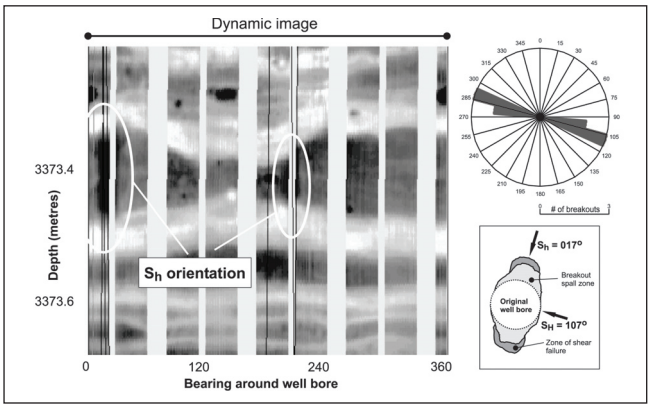

Fig. 2. Borehole breakouts from the Mutineer 1b image log showing the azimuth (orientation) of S_h. Rose diagram shows the azimuth of S_H interpreted from Mutineer 1b breakouts.

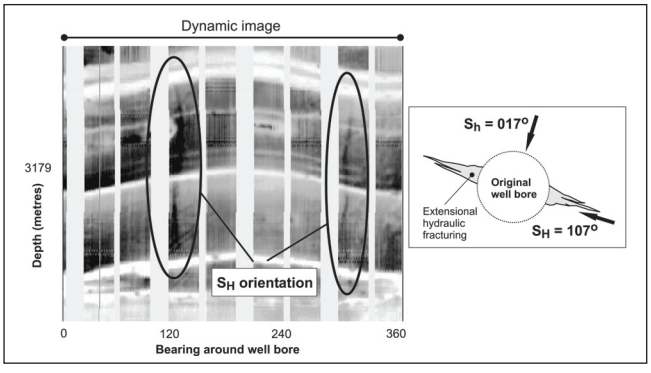

Fig. 3. Drilling-induced tensile fractures from the Mutineer 1b image log showing the azimuth (orientation) of S_H.

Horizontal stress orientations were obtained from borehole breakouts and DITFs. Breakouts are intervals where the well bore develops an elliptical cross-section due to failure of the well bore wall (Zoback et al., 1985). Drilling a vertical well bore in a body of rock disturbs the stress field. Compressive "hoop" stresses acting around the well bore become maximised at the azimuth of S_h. If the stresses exceed the compressive strength of the formation, shear failure occurs and pieces of wall rock break away. The result is that the well bore develops an elliptical cross-section with the long axis of the ellipse aligned parallel to S_h in vertical wells. Breakouts on image logs manifest as relatively wide, conductive (dark) features due to the infiltration of conductive drilling mud into the damage zone (Figure 2). A combination of these dark features appearing on opposing pads and caliper mismatches set the criteria for interpreting breakouts. Drilling-induced tensile fractures develop orthogonal to breakouts and therefore propagate parallel to S_H (Hillis and Williams, 1993). Tensile fracturing requires the minimum stress concentration around the well bore to be equal to, or less than, zero at the azimuth of S_H. They appear as narrow dark lines on image logs (Figure 3). Drilling-induced tensile fractures in vertical wells, like borehole breakouts, develop where there are large anisotropies between the maximum and minimum horizontal stresses. Descriptions of the formation of breakouts and DITFs can be found in Moos and Zoback (1990). Descriptions of the interpretation of stress directions from log information can be found in Plumb and Hickman (1985) and Aadnøy and Bell (1998).

The only well with an image log is Mutineer 1b and small, poorly developed breakouts are seen on this log (Figure 2). Breakouts indicate that S_h has an average azimuth of 017°N therefore S_H is orientated 107°N. Incipient DITFs are also seen on the Mutineer 1b image log (Figure 3). In all bar one instance, DITFs occur on one pad of the FMI tool thus creating difficulty in interpreting the orientation of S_H. However, their presence is used

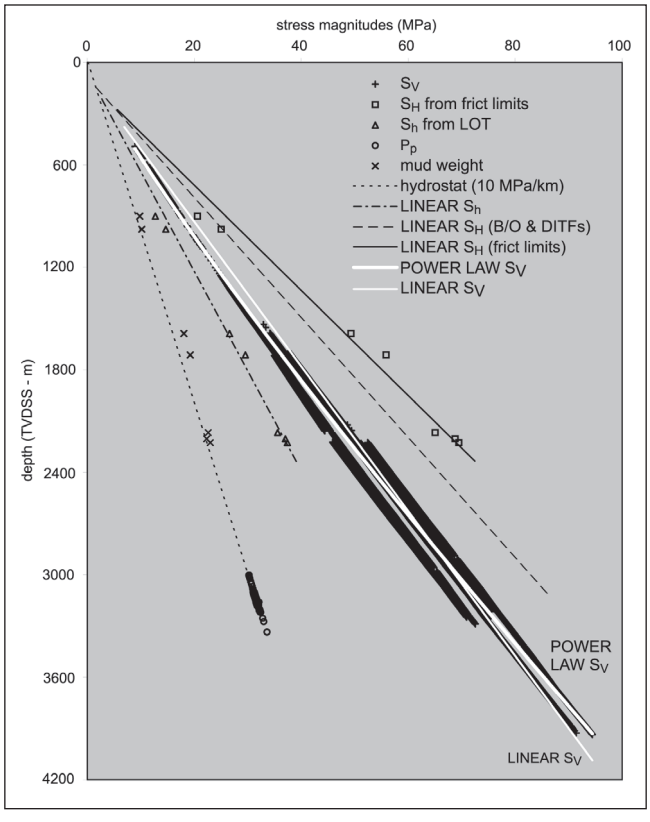

Fig. 4. Stress versus depth plot for Mutineer-Exeter.

in the calculations of S_H magnitude. Determined horizontal stress orientations closely match those orientations interpreted from borehole breakouts by Hillis and Williams (1993) for the Wanaea-Cossack fields located 50 km to the SW of Mutineer-Exeter. An average S_H orientation of 110°N was determined for these fields.

VERTICAL STRESS (S_V) MAGNITUDE

The true vertical stress (S_V) at a specified depth (z) is defined as the pressure exerted by the weight of all overlying rocks (Engelder, 1993). At depth z, it is expressed as the integral of the average bulk density of overlying rocks (ρ_b) and gravity (g):

$$S_V = \int_0^z z\rho_b g.dz \ . \qquad (1)$$

Accurate knowledge of the density of the overlying rock column is required to calculate S_V. A commonly made assumption is that S_V increases with depth at a rate of 1 psi/ft or 22.6 MPa/km (Matthews and Kelly, 1967; Gaarenstroom et al., 1993). The approximation comes from assuming that rocks have an average bulk density of 2.3 g/cc. While this more or less holds, there are documented examples where S_V increases from 0.8 psi/ft at shallow depths to over 1.1 psi/ft in deeper, well-compacted sections (Hillis et al., 1998). The increase in gradient occurs because sediments become more compacted with depth and their densities increase. Hence, it is likely that the S_V gradient varies both between basins and with depth in the same basin.

Actual S_V profiles are calculated using density log data from Mutineer-Exeter. Those data where the density correction (DRHO) exceeded 0.05 g/cc were removed from the data set to ensure that only reliable data were used. Further filtering of the data reduced the number to a manageable amount and removed outlying points. Density logs are not commonly recorded from the seabed, therefore to ensure the accuracy of the S_V profile the average density of the sediments from the seabed to the top of the density log was estimated. This was done using the Nafe-Drake transform for sedimentary rocks to convert compressional wave (sound) velocity data to density. The Nafe-Drake transform relies on the correlation between sediment density and sonic velocity (Ludwig et al., 1970). It is derived empirically from sonic and density log data and laboratory measurements of core samples. Correlations are then re-calibrated for each individual well by cross-plotting all density and sonic data and laterally shifting the Nafe-Drake curve to pass through the average sonic velocity/density value. The re-calibrated correlation was then used to convert average velocity at the top of the density log to an average density (Tingay et al., 2003). All data from the wells are plotted versus depth from the sea surface to create a S_V profile relevant to the whole of Mutineer-Exeter (Figure 4). An average water depth of 150 metres was assumed with an average water density of 1.03 g/cc. The S_V profile is best described by a power law function:

$$S_V(MPa) = 0.0076 \times depth(m)^{1.1389} \ . \qquad (2)$$

The software used to perform the geomechanical modelling to assess the risk of fault reactivation requires a generic linear S_V profile. While not as good a fit as the power law function in equation (2), the Mutineer-Exeter vertical stress profile can be approximated as:

$$S_V(MPa) = 0.0236 \times depth(m) - 2.0000 \ . \qquad (3)$$

MINIMUM HORIZONTAL STRESS (S_h) MAGNITUDE

The most reliable determinations of S_h are derived from hydraulic fracturing tests (Engelder, 1993). Unfortunately, these tests are not widely performed during exploration drilling. However, pumping pressure tests are commonly conducted. This study uses a compilation of leak-off pressures (LOPs) from single-cycle leak-off tests (LOTs) from all the wells to calculate S_h. During these tests, the pressure at which a fracture in the well bore opens is recorded. Hence, the aim is to assess the fracture strength of the rock unit immediately beneath a newly set casing in a well (Bell, 1990). The basic LOT technique involves drilling several metres beneath the base of the casing and pumping drilling mud into the well bore while monitoring surface pump pressures for indications of formation failure. The pumping of drilling mud into the well bore drives the pressure beyond that of the static mud column resulting in elastic expansion of the uncased hole. The LOP is reached when the increase in pressure with volume of mud pumped deviates from a linear relationship. At this point, the gradient of the pressure versus volume of mud pumped graph will decrease as mud escapes into the formation below the casing along pressure-induced tensile fractures. Subsequent to leak-off, pumping ceases and well-bore mud pressures are allowed to decay back to those exerted by the static mud column. For a more detailed description of the LOT technique, see Bell (1990) and White et al. (2002).

Leak-off pressures are controlled by the disturbed stress field at the well bore wall, and contain a component of the formation tensile strength. Hence, they do not provide as reliable estimates of S_h as hydraulic fracturing test measurements, for example. Nevertheless, it is commonly accepted that the lower bound to LOPs provides a reasonable estimate for S_h (Breckels and van Eekelen, 1982; Gaarenstroom et al., 1993). For the Mutineer-Exeter data however, a linear function provides the best fit:

$$S_h(MPa) = 0.0171 \times depth(m) - 1.0000 \ . \qquad (4)$$

The trend is fitted so S_h is equal to the hydrostatic pressure at the seabed. The increase in S_h with depth below the seabed is 17.1 MPa/km. The absence of data from greater than 2500 m means the magnitude of S_h is poorly constrained for the reservoir interval (~ 3000 m). This is because pumping pressure tests from these depths were formation integrity tests where leak-off was not achieved. Formation integrity values, which comprised 15 of the 22 pumping pressure values, are not used in the calculations (or in subsequent calculations of S_H) because they under-estimate S_h (White et al., 2002). Hence, a projection of the LOT data from more shallow depths constrains S_h through the reservoir interval. The available data show $S_h < S_V$ implying the stress regime is either normal ($S_h < S_H < S_V$) or strike-slip ($S_h < S_V < S_H$).

MAXIMUM HORIZONTAL STRESS (S_H) MAGNITUDE

The maximum horizontal stress (S_H) is the most difficult to quantify of the principal stresses as it cannot be measured directly. A maximum value for S_H is calculated using the frictional limits to stress algorithm (Jaeger and Cook, 1979). The algorithm quantifies S_H by assuming it is the maximum principal stress (S_1). The approach is valid as long as the coefficient of sliding friction (μ) is not so great as to inhibit motion on optimally orientated pre-existing faults (Zoback and Healy, 1984). For optimally orientated faults, the ratio of maximum to minimum effective stress ($\sigma_1' : \sigma_3'$) at which slip will occur is described by:

$$\frac{\sigma_1'}{\sigma_3'} = \left(\sqrt{(\mu^2+1)} + \mu\right)^2 \ . \qquad (5)$$

Optimally orientated faults concur with Andersonian theory and hence strike at 30° to S_1 (in this case S_H) and are vertical. They are typically assumed to have Byerlee μ values of 0.6 to 0.85 and to be

cohesionless (Byerlee, 1978). If the $\sigma_1' : \sigma_3'$ ratio is less than the function of μ then all faults should be stable and no slip will occur. If the ratio is exactly this value, slip will only occur on optimally orientated fault planes. The frictional limit for S_H calculated using $\mu = 0.6$ together with measurements of S_h determined from LOTs and virgin P_p has the equation:

$$S_H(MPa) = 0.0323 \times depth(m) - 3.2500 \quad . \qquad (6)$$

The frictional limit to S_H has a gradient of 32.3 MPa/km (Figure 4). More accurate determinations of S_H can be made, given the presence of borehole breakouts and DITFs (Moos and Zoback, 1990; Peska and Zoback, 1995). Their occurrence on the image log from Mutineer 1b was combined with rock strength data (from multiple stage triaxial testing), orientations and magnitudes of the other principal stresses, pore pressure data and mud weights from that well. Stress concentrations at all angles relative to the known azimuth of S_H (θ) around a vertical well bore can be described in terms of the far field stress tensor, P_p and the mud weight (Moos and Zoback, 1990):

$$S_{\theta\theta} = S_H + S_h - 2(S_H - S_h)\cos 2\theta - weight_{mud} - P_p \quad . \qquad (7)$$

The magnitude of S_H is the only unknown component required to calculate the stress concentration. Therefore its value in equation (7) can be maximised so that the circumferential stress concentration ($S_{\theta\theta}$) around the well bore is both less than the tensile strength of the wall rock to create DITFs and in excess of the compressive strength, thus forming breakouts. In this way it is possible to determine a value of S_H for which rock failure occurs. The approach is dependent on knowledge of the compressive and tensile strengths of the wall rock. However, by assuming that there are pre-existing fractures within a given body of rock the tensile strength can be considered negligible, as fractures will re-open at stresses lower than those required to create new ones. An estimate for S_H was made given the presence of incipient borehole breakouts and DITFs in Mutineer 1b and using the modified Lade Criterion (Ewy, 1998). The calculation can be further constrained by the ratio between S_h and S_V at the depth where the Mutineer 1b rock mechanical testing samples were retrieved (3100 m). At this depth in this well the ratio of the projection of LOT data normalised to the power law S_V curve is 0.766 (Figure 5). Therefore it is inferred that the increase in S_H with depth is 28.6 MPa/km (Figure 4):

$$S_H(MPa) = 0.0286 \times depth(m) - 2.779 \quad . \qquad (8)$$

Knowledge of the stress magnitudes and orientations constrains the tectonic regime. Leak-off test data show that the minimum principal stress in Mutineer-Exeter is horizontal. Modelling of the magnitude of S_H shows that the regional maximum principal stress is also horizontal. It is therefore inferred that the tectonic regime is strike-slip ($S_h < S_V < S_H$). The allowable regions diagram (Figure 5) shows the relationship between the principal stresses at 3100 m for Mutineer 1b. The same relationship was inferred for the whole of Mutineer-Exeter. The *x*-axis shows the minimum horizontal to vertical stress ratio and the *y*-axis shows the maximum horizontal to vertical stress ratio. The outer lines represent frictional limits ($\mu = 0.6$). Breakout and DITF lines indicate the stress states required for each to form.

Stress	Gradient (MPa/km)	Orientation (°N)
S_V	23.6	Vertical
S_H	28.6	107
S_h	17.1	017

Table 1. Principal stress gradients (shown in Figure 4) and orientations used in the geomechanical modelling of fault reactivation risk.

GEOMECHANICAL MODELLING OF FAULT REACTIVATION RISK

Geomechanical modelling assesses the likelihood of reactivation of pre-existing faults. These faults within Mutineer-Exeter are of Jurassic–Cretaceous age, have predominant orientations of NE–SW and dip between 10° and 60° to both the SE and NW (Figure 6). They show little or no offset of the overlying Tertiary. Faults tip out vertically around 3 km depth and penetrate as deeply as 6 km. Fault reactivation has the potential to breach fault bounded hydrocarbon traps regardless of fault juxtaposition and/or a fault

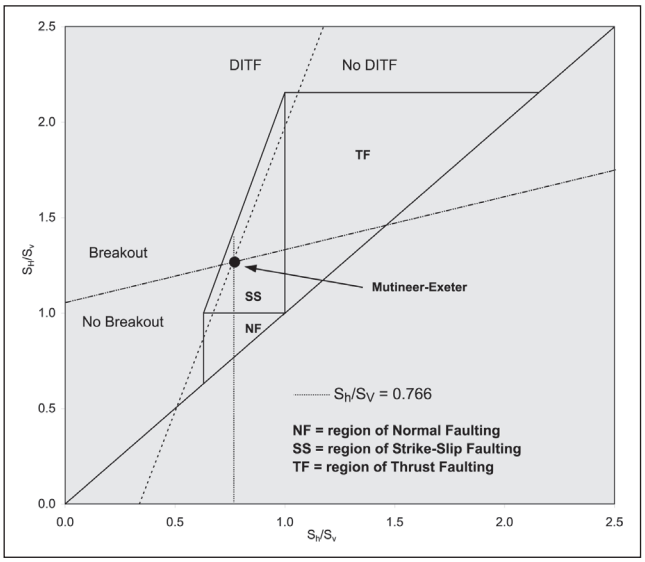

Fig. 5. Allowable regions diagram for Mutineer 1b showing the relationship between the principal stresses.

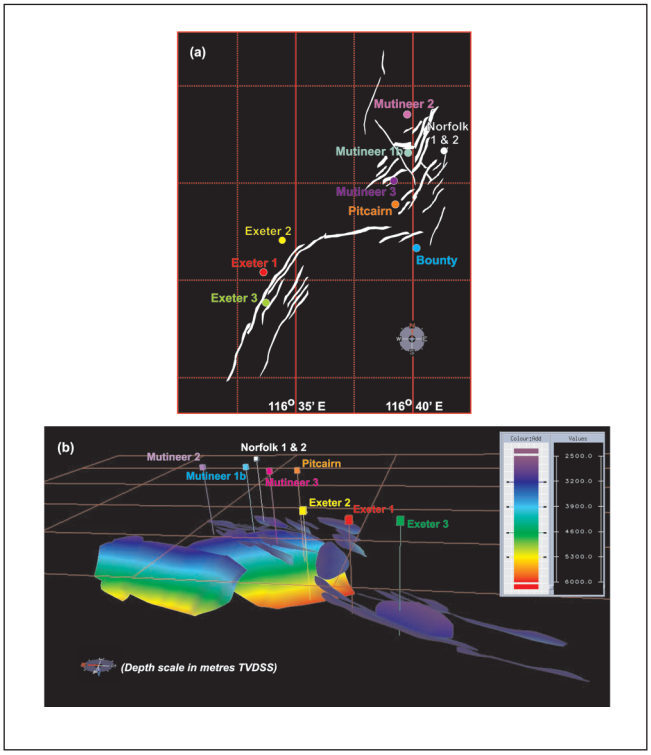

Fig. 6. Fault orientations across Mutineer-Exeter in (a) map view and (b) perspective view coloured for depth (red grid represents sea level).

damage-related seal. Indeed, there is a growing body of evidence to suggest that active faults (those subjected to stresses that can induce failure) strongly influence fluid flow within hydrocarbon reservoirs (Smith, 1980; Sibson, 1994; Matthäi et al., 1998).

Geomechanical modelling requires a regional pore pressure profile and stress tensor, summarised in Table 1, together with fault information. A stipulation of the modelling software used to assess reactivation risk, *TrapTester*, is that the principal stress magnitudes increase linearly with depth. Table 1 therefore summarises the gradients for S_h, S_H, and S_V from Figure 4 that are input into the geomechanical model. *TrapTester* is a commercial software package developed by Badleys (<www.badleys.co.uk>), and a brief outline of the modelling approach is given below. For a more complete description of the methodology used by *TrapTester* (previous incarnations were known as FAPS) for fault modelling, readers are directed towards Freeman et al. (1998) and Yielding et al. (1999).

The technique used to create the geomechanical model in *TrapTester* involves first importing geological information in the form of fault and horizon surfaces, interpreted from seismic cross sections. Fault traces on mapped horizon surfaces and fault profiles from seismic slices are used to define positions of fault surfaces in 3-dimensional space. The picks of each point on a fault are typically stored as XYZ data points, where X and Y are longitude and latitude and Z is depth. Each fault surface is modelled as a 3-dimensional grid, the principal axes of the grid being parallel to the strike and dip of the fault, using a grid mesh size defined by the user. The grid produces an accurate representation of the shape and orientation of the fault, and is used as the base on which to calculate a variety of attributes (Yielding et al., 1999).

TrapTester is not a finite-element modelling package. Modelling results can only be influenced by the values of the input stress tensor and pore pressure profile. The software calculates the stress at any point on the fault surface using the predetermined stress tensor and pore pressure profile. Consistent stress magnitudes and orientations are assigned to the whole of Mutineer-Exeter (Table 1). Different pore pressure profiles can be built into the hanging wall and footwall sides of faults, and compartments of overpressure, for example, can be incorporated using the horizon surfaces. However, using the data displayed in Figure 4, a hydrostatic pore pressure profile was assumed throughout the region. Fault reactivation risk is assessed using a Mohr-Coulomb shear failure envelope with a frictional angle of 30° corresponding to a coefficient of friction (μ) of 0.6. *TrapTester* also assumes that pre-existing faults have cohesionless fault surfaces (C_0 is zero), an assumption that is probably slightly unrealistic in nature.

Fault reactivation risk assessments are based on a reduction in effective stress and hence quantified as the change in pore pressure that would induce failure. This way of quantifying reactivation is not meant to imply that failure is always due to increases in pore pressure such as fluid injection into the reservoir. It merely provides a simple way of expressing the proximity of a fault plane of any orientation to the shear failure envelope. Brittle failure is therefore predicted if the increase in pore pressure (ΔP_p) causes the Mohr circle to intersect the failure envelope (Figure 7). Faults most at risk of reactivation require a smaller ΔP_p to induce movement (Mildren et al., 2002). *TrapTester* colours fault segments according to the ΔP_p required to bring about slip. Figure 8 shows the risk of fault reactivation. Reactivation has the greatest implication through the reservoir interval (~ 3100 metres in Figure 6) but fortunately the likelihood of reactivation is mainly low to moderate. Most faults are non-optimally orientated for slip to occur. Those fault segments most susceptible to reactivation strike NW–SE.

The Fault Analysis Seal Technology, or FAST, polar plot represents the orientation of all possible faults plotted as poles to planes (Figure 9). FAST calculations are the same as the *TrapTester* reactivation risk calculations since *TrapTester* uses the FAST algorithm to calculate ΔP_p. A description of the FAST technique can be found in Mildren et al., 2002. Figure 9 shows the reactivation risk of all possible faults at the depth of the Angel (reservoir) Sandstone. Hot colours represent high-risk fault orientations (low ΔP_p) while cold colours represent a lower risk (high ΔP_p). The dark arcs indicate the orientation of the Mutineer-Exeter faults. Existing fault orientations contrast with fault orientations optimal for reactivation. Optimal orientations are sub-vertical and have strikes of around 080°N and 135°N. These strikes follow Andersonian theory by being aligned 30° to the azimuth of S_H. Therefore, hydrocarbon traps requiring these

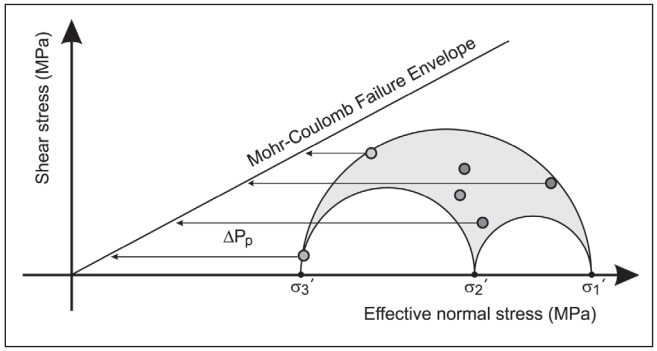

Fig. 7. Three-dimensional Mohr diagram and Mohr-Coulomb failure envelope. Faults of all possible orientations plot within the shaded region. The horizontal distance between the fault plane and the failure envelope (ΔP_p) describes the likelihood of fault reactivation.

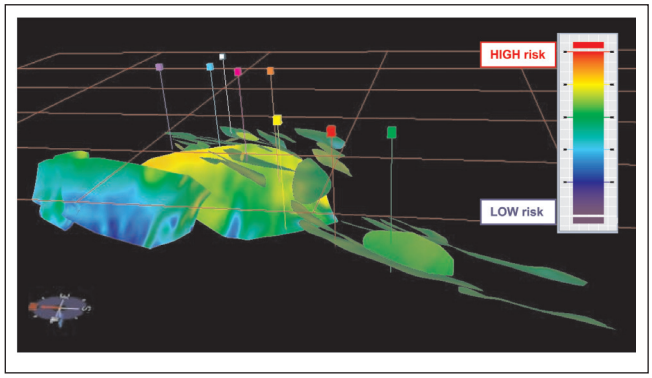

Fig. 8. Three-dimensional image showing the risk of reactivation for the Mutineer-Exeter faults.

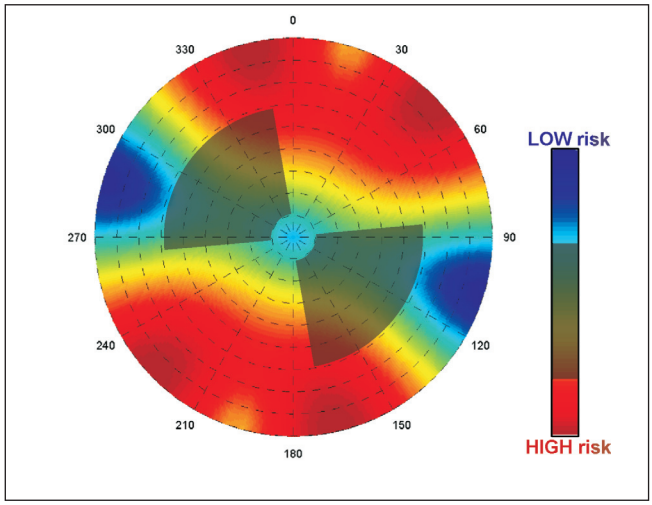

Fig. 9. Reactivation risk assessed for all possible fault orientations (dark arcs represent Mutineer-Exeter faults).

faults to be sealing are most likely to be breached given the in-situ stress field.

A ΔP_p can lead to the creation of new faults, especially when existing faults are non-optimally orientated for reactivation. The type of fracture formed is controlled by the stress magnitudes and the strength of the rock. Modelling shows that the creation of new faults requires a greater ΔP_p than reactivation, because intact rock has a material strength in excess of that of a fault. Thus, the intact rock failure envelope will plot to the left of the fault rock failure envelope on a Mohr diagram. New faults are most likely to be shear structures.

DISCUSSIONS AND IMPLICATIONS

TrapTester calculates the risk of fault reactivation with a change in pore pressure, ΔP_p. An increase in P_p is the usual cause of fault reactivation as it reduces the effective stresses, driving the Mohr circle towards the failure envelope. In the case of Mutineer-Exeter, production will lead to a reduction in P_p. Therefore, the Mohr circle will move away from the failure envelope, reducing the susceptibility of fault reactivation.

Reactivation in Mutineer-Exeter is unlikely for other reasons. First, the majority of faults are non-optimally orientated. Non-optimally orientated faults require greater changes in effective stress magnitude (hence ΔP_p) to cause slip. In addition, there is no documented evidence of damage to well bore casings due to fault reactivation. The authors are also unaware of any leakage indicators, either on the seabed or the sea surface, such as those detected by remote sensing methods (e.g., O'Brien et al., 1998). Second, data suggest that the tectonic regime is strike-slip. Therefore both S_1 and S_3 are horizontal, meaning that failure due to pore pressure-stress coupling is probably not an issue (see Hillis, 2003). Unfortunately, there are no data known to the authors that document the changes in S_H with ΔP_p. Thus, the behaviour of the full stress tensor for a given ΔP_p remains unconstrained. It is believed that coupling affects both horizontal stresses in the same way meaning the diameter of the Mohr circle remains fixed. Yassir and Rogers (1993) suggest that S_H increases similarly to S_h with a positive ΔP_p. It is therefore prudent to suggest S_H decreases similarly to S_h with a negative ΔP_p. However, given the lack of data, hypotheses such as these are speculative.

The creation of new fractures during production is also unlikely. The relatively high rock strength is believed to prevent them (Tan, pers. comm., 2003). Ekofisk, in the Norwegian North Sea, is a large chalk reservoir where production drawdown was up to 24 MPa. The large drawdown was especially significant when paired with an inherent structurally weak chalk matrix (Teufel et al., 1991). This contrasts to the strong sandstone matrix of the Mutineer-Exeter Angel Formation. Another important aspect of the Ekofisk chalk was the initially high porosity of up to 50%. As Teufel et al. (1991) state, this high porosity was one of the reasons why shear failure occurred. Virgin pore pressures within Mutineer-Exeter are hydrostatic, thus implying the reservoir has undergone normal sediment compaction. This again contrasts with the Ekofisk field that had an initial reservoir overpressure magnitude of 17 MPa (Hermansen et al., 2000). Significant overpressures such as these contributed to the excess porosity that in turn would contribute to the structural weakness of the reservoir. Normally compacted rocks and high rock strengths in Mutineer-Exeter should also remove many of the risks associated with poro-elastic compaction of the reservoir. Compaction results in subsidence that can induce permanent damage to top and fault seals.

CONCLUSIONS

Hydrocarbon production results in pore pressure drawdown, a process that can potentially reactivate existing faults or create new faults in a region. Evaluations of the likelihood of fault reactivation require detailed information about the in-situ stress field and the location of faults. It is also required to know pore pressures prior to production and mechanical properties of seal and reservoir rocks.

The stress field was determined using exploration well data. Borehole breakouts and incipient drilling-induced tensile fractures (DITFs) give a S_H orientation of 107°N, consistent with data from surrounding regions. Stress magnitude estimates show that the tectonic regime in Mutineer-Exeter is strike-slip ($S_h < S_V < S_H$).

The risk of fault reactivation in Mutineer-Exeter was assessed using *TrapTester*, rock mechanical data, the in-situ stress field, and a hydrostatic P_p profile. Geomechanical modelling shows that the likelihood of reactivation is low to moderate. Faults most likely to be reactivated would be sub-vertical and have orientations of 080°N and 135°N. There are no faults with these orientations within Mutineer-Exeter. Subsequent modelling assessed the likelihood of new fault formation. The stress field and the frictional and cohesive strengths of the rock control the type of fault formed. Larger ΔP_p magnitudes are required to create new faults than to reactivate existing structures.

ACKNOWLEDGEMENTS

The authors thank Santos for the provision of well and fault data and permission to publish. Chee Tan (CSIRO) and Tom Chapman (Santos) are thanked for the rock mechanical data. Jerry Meyer (JRS Petroleum Research) is thanked for help with image log interpretation and the determination of S_H. This study forms part of an ARC Linkage Project involving the Australian School of Petroleum, the University of Western Australia, Santos, Woodside, and Agip/ENI Australia.

REFERENCES

Aadnøy, B., and Bell, J.S., 1998, Classification of drilling-induced fractures and their relationship to *in-situ* stress direction: *The Log Analyst*, **39**, 27–42.

Bell, J.S., 1990, Investigating stress regimes in sedimentary basins using information from oil industry wireline logs and drilling records: in Hurst et al. (eds.), *Geological Applications of Wireline Logs*: Geological Society of London Special Publication, **48**, 305–25.

Breckels, I.M., and van Eekelen, H.A.M., 1982, Relationship between horizontal stress and depth in sedimentary basins: *Journal of Petroleum Technology,* **34**, 2191–9.

Byerlee, J., 1978, Friction of Rocks: *Pure and Applied Geophysics*, **116**, 615–26.

Engelder, T., 1993, *Stress Regimes in the Lithosphere*: Princeton University Press.

Ewy, R.T., 1998, Well bore stability predictions using a modified Lade Criterion: *SPE/ISRM Eurock '98*, Trondheim, Norway, 8th–10th July 1998. ***SPE* 47251**.

Freeman, B., Yielding, G., Needham, D.T., and Badley, M.E., 1998, Fault seal prediction: the gouge ratio method: in Coward et al. (eds.), *Structural Geology in Reservoir Characterisation*: Geological Society of London Special Publication, **127**, 19–25.

Gaarenstroom, L., Tromp, R.A.J., de Jong, M.C., and Brandenburg, A.M., 1993, Overpressures in the Central North Sea: implications for trap integrity and drilling safety: in Parker, J.R. (ed.), *Petroleum Geology of NW Europe: Proceedings of the 4th Conference.* Geological Society of London, 1305–1313.

Hermansen, H., Landa, G.H., Sylte, J.E., and Thomas, L.K., 2000, Experiences after 10 years of waterflooding the Ekofisk Field, Norway: *Journal of Petroleum Science & Engineering*, **26**, 11–18.

Hillis, R.R., 2003, Pore pressure/stress coupling and its implications for rock failure: in van Rensbergen et al. (eds.), *Subsurface Sediment Mobilisation*: Geological Society of London Special Publication, **216**, 359–68.

Hillis, R.R., and Williams, A.F., 1993, The contemporary stress field of the Barrow-Dampier Sub-basin and its implications for horizontal drilling: *Exploration Geophysics*, **24**, 567–76.

Hillis, R.R., Meyer, J.J., and Reynolds, S.D., 1998, The Australian stress map: *Exploration Geophysics,* **29**, 420–27.

Jaeger, J.C., and Cook, N.G.W., 1979, *Fundamentals of Rock Mechanics (3rd Edition)*: Chapman & Hall, London.

Ludwig, W.E., Nafe, J.E., and Drake, C.L., 1970, Seismic refraction: in Maxwell, A.E. (ed.), *The Sea: Ideas and Observations on Progress in the Study of the Seas*, **4 #1**, 53–84: Wiley Interscience, New York.

Matthäi, S.K., Aydin, A., Pollard, D.D., and Roberts, S.G., 1998, Numerical simulation of departures from radial drawdown in a faulted sandstone reservoir with joints and deformation bands: in Jones et al. (eds.), *Faulting, Fault Sealing and Fluid Flow in Hydrocarbon Reservoirs*: Geological Society of London Special Publication, **147**, 157–91.

Matthews, W., and Kelly, J., 1967, How to predict formation pressure and fracture gradient: *Oil & Gas Journal*, **65**, 92–106.

Mildren, S.D., Hillis, R.R., and Kaldi, J., 2002, Calibrating predictions of fault seal reactivation in the Timor Sea: *APPEA Journal*, **42 #1**, 187–202.

Moos, D., and Zoback, M.D., 1990, Utilisation of Observations of Well Bore Failure to Constrain the Orientation and Magnitude of Crustal Stresses: Application to Continental, Deep Sea Drilling Project and Ocean Drilling Program Boreholes: *Journal of Geophysical Research*, **95 #B6**, 9305–25.

O'Brien, G.W., Quaife, P., Cowley, R., Morse, M., Wilson, D., Fellows, M., and Lisk, M., 1998, Evaluating trap Integrity in the Vulcan Sub-basin, Timor Sea, Australia, using Integrated Remote-Sensing Geochemical Technologies: in Purcell, P.G., and Purcell, R.R. (eds.), *The Sedimentary Basins of Western Australia 2. Proceedings of the PESA Symposium*, 237–54.

Peska, P., and Zoback, M.D., 1995, Compressive and tensile failure of inclined well bores and determination of *in-situ* stress and rock strength: *Journal of Geophysical Research,* **100**, 12791–811.

Plumb, R.A., and Hickman, S.H., 1985, Stress-induced borehole elongation: a comparison between 4-arm dipmeter and the borehole televiewer in the Auburn geothermal well: *Journal of Geophysical Research*, **90**, 5513–21.

Sibson, R.H., 1994, Crustal Stress, Faulting and Fluid Flow: in Parnell, J. (ed.), *Geofluids: Origin, Migration and Evolution of Fluids in Sedimentary Basins*: Geological Society of London Special Publication, **78**, 69–84.

Smith, D.A., 1980, Sealing and non-sealing faults in Louisiana Gulf Coast Salt Basin: *AAPG Bulletin*, **64**, 145–72.

Streit, J.E., and Hillis, R.R., 2002, Estimating fluid pressures that can induce reservoir failure during hydrocarbon depletion: *SPE/ISRM Rock Mechanics Conference*, Irving, Texas, 20th–23rd October 2002.

Teufel, L.W., Rhett, D.W., and Farrell, H.E., 1991, Effect of reservoir depletion and pore pressure drawdown on *in-situ* stress and deformation in the Ekofisk Field, North Sea: *Proceedings of 32nd U.S. Symposium on Rock Mechanics*, Balkema, 63–72.

Tingay, M.R.P., Hillis, R.R., Morley, C.K., Swarbrick, R.E., and Okpere, E.C., 2003, Variation in vertical stress in the Baram Basin, Brunei: tectonic and geomechanical implications: *Marine & Petroleum Geology*, **20**, 1201–1212.

White, A.J., Traugott, M.O., and Swarbrick, R.E., 2002, The use of leak-off tests as means of predicting minimum *in-situ* stress: *Petroleum Geoscience*, **8 #2**, 189–93.

Yassir, N.A., and Rogers, A.L., 1993, Overpressures, fluid flow and stress regimes in the Jeanne D'Arc Basin, Canada: *International Journal of Rock Mechanics, Mining Sciences and Geomechanical Abstracts*, **30 #7**, 1209–13.

Yielding, G., Øverland, J.A., and Byberg, G., 1999, Characterisation of Fault Zones for Reservoir Modelling: An Example from the Gullfaks Field, Northern North Sea: *AAPG Bulletin*, **83**, 925–51.

Zoback, M.D., and Healy, J., 1984, Friction, faulting and *in-situ* stress: *Annales Geophysicae*, **2**, 689–98.

Zoback, M.D., Moos, D., Mastin, N., and Anderson, R.L., 1985, Well bore breakouts and *in-situ* stress: *Journal of Geophysical Research*, **90**, 5523–30.